The Journal of Cosmology

Journal of Cosmology, 2011, Vol 13, In Press.
JournalofCosmology.com, 2011

Observational Evidence Favors a Static Universe

Part 2

David F. Crawford
Sydney Institute for Astronomy,
School of Physics, University of Sydney.
NSW, Australia

ABSTRACT

This is the second part (of a three part report) which covers the topics: X-ray background radiation, cosmic background microwave radiation, dark matter, Sunyaev–Zel'dovich effect, gravitational lensing, Lyman- forest, nuclear abundances, galactic rotation curves, redshifts in our Galaxy, anomalous redshifts and voids. An analysis of the best raw data for these topics shows that, in general, they are consistent with both Big Bang cosmology and curvature cosmology. It is shown that the Xray data in the range from about 10 Kev to about 300 kev can be explained by bremsstrahlung from the cosmic gas with a fitted temperature of $2.62 \pm 0.04 \times 10^9$ K whereas the predicted temperature is 2.56×10^9 K showing excellent agreement. The fitted density was $N = 1.55 \pm 0.01$ hydrogen atoms per cubic meter (2.57×10^{-27} kgm^{-3}) from which CC predicts a Hubble constant of $H = 64.4 \pm 0.2$kms^{-1} Mpc^{-1}. A further prediction by CC is a temperature of 3.18K for the cosmic microwave background radiation. Whereas the conclusions in Part 1 would be valid for any reasonable static cosmology the analysis in Part 2 requires specific characteristics of curvature cosmology.

Keywords: Big Bang, Infinite Universe, Steady State Universe, Static Universe, Expanding Universe

Observational evidence favors a static universe
Part 2

1 Introduction

Apart from its lack of expansion, curvature cosmology (CC) makes further specific predictions that can be compared with BB. These are considered in this Part. Whereas the conclusions about expansion and evolution in Part 1 would be applicable for any reasonable static cosmology this section considers topics that depend specifically on CC.

The topic of X-ray background radiation is very important for CC. Not only can CC explain the radiation from 10–300 keV but the results enable estimates for the temperature and density of the cosmic gas (the gas external to clusters of galaxies). It is shown that the X-ray data in the range from about 10 Kev to about 300 kev can be explained by bremsstrahlung from the cosmic gas. The fitted temperature was $2.62 \pm 0.04 \times 10^9$ K whereas the predicted temperature is 2.56×10^9 K showing excellent agreement. The fitted density was $N = 1.55 \pm 0.01$ hydrogen atoms per cubic meter (2.57×10^{-27} kg m^{-3}).

In CC the CMBR is produced by very high energy electrons via curvature-redshift radiation in the cosmic plasma. The predicted temperature of the CMBR is 3.18 K to be compared with an observed value of 2.725 K (Mather et al., 1990). The prediction does depend on the nuclei mix in the cosmic gas and could vary from this value by several tenths of a degree. It is argued that in CC the observed larger CMBR temperature at large redshifts could be explained by the effects of curvature redshift on the width of spectral lines. Evidence for

correlations between CMBR intensity and galaxy density is consistent with CC.

Regarding dark matter not only does CC have a quite different explanation for the redshift dispersion in clusters of galaxies but it can make a good estimate, without any free parameters, of its value for the Coma cluster. In BB it is assumed that the redshift dispersion is a genuine velocity dispersion and the mass of a cluster of galaxies is determined by using the virial theorem. In CC the redshift dispersion is due to effects of curvature redshift produced by the intra-cluster gas.

The Sunyaev–Zel'dovich effect, gravitational lens, the Lyman-α forest and the Gunn–Peterson trough can be explained by or are fully consistent with CC. BB offers a good explanation for the primordial abundances of the light nuclei, albeit with some uncertainty of the density of the early universe at their time of formation. In CC the distribution of light elements is determined by nuclear reactions in cosmic gas that has a similar very high temperature. This explanation needs a quantitative analysis.

Galactic rotation curves are a problem for both cosmologies. BB requires an extensive halo of dark matter around the galaxy while CC requires a reasonable halo of normal matter to produce the apparent rotation via curvature redshift. Its problem is getting the required asymmetry in the halo distribution.

Anomalous redshifts are the controversial association of high redshift quasars with much lower redshift galaxies. Although they are inexplicable in BB, CC could offer a partial explanation for some observations.

Finally voids and other large scale structures in the redshift distribution of quasars and galaxies is easily explained in CC by the extra redshift due to curvature redshift in higher density gas clouds. In BB it is a complicated result

of the evolution of these objects.

2 Non-expansion Observations

2.1 The Hubble redshift

The increase in the redshift of an object with distance is well documented and both cosmologies provide a solution. In BB it is due to the expansion of the universe which is predicted by general relativity. The basic instability of the Einstein model is well known (Tolman, 1934; Ellis, 1984). Although the inclusion of a cosmological constant provides a static solution it is still unstable and after a small perturbation will either expand or contract. Thus the BB is in full agreement with general relativity. On the other hand in CC the Hubble redshift is due to a gravitational interaction between the photons and the cosmic gas whose density produces a curved space-time. Both cosmologies predict that for nearby distances the Hubble redshift is a linear function of distance. However in CC it depends on the integral of the square root of the density along the path length and can because of density variations in a particular situation it may vary from the average value. Another important difference is that CC predicts the actual value for the Hubble constant. For the measured density of $N = 1.55 \pm 0.01\,\mathrm{m}^{-3}$ the calculated value of the Hubble constant is $H = 64.4 \pm 0.2\,\mathrm{km\,s}^{-1}\,\mathrm{Mpc}^{-1}$ whereas the value estimated from the type 1a supernova data (in Part 1) is $63.8 \pm 0.5\,\mathrm{kms}^{-1}$ Mpc^{-1} and the result from the Coma cluster (Section 2.15) is $65.7\,\mathrm{kms}^{-1}$ Mpc^{-1}.

2.2 X-ray background radiation

Since Giacconi et al. (1962) observed the X-ray background there have been many suggestions made to explain its characteristics. Although much of the unresolved X-ray emission comes from active galaxies, there is a part of the spectrum between about 10 keV and 1 MeV that is not adequately explained by emission from discrete sources. The very high energy range is most likely due to external point sources. It is the intermediate range that is examined here.

2.2.1 X-rays in BB

In Big-Bang cosmology for the intermediate X-ray range of about 10–300 keV, the production of X-rays in hot cosmic plasma through the process of bremsstrahlung has been suggested by Hoyle & Narliker (1962); Gould & Burbidge (1963); Field & Henry (1964); Cowsik & Kobetich (1972). In a review of the spectrum of the X-ray background radiation Holt (1992) concluded that the measured spectra of discrete sources are not consistent with the observations in the intermediate energy range but there is a remarkable fit to a 40 keV (4.6×10^8 K) bremsstrahlung spectrum from a diffuse hot gas. However, in an expanding universe most of the X-rays are produced at redshifts of $z \geqslant 1$ where the density is large enough to scatter the CMBR. This scattering known as the Sunyaev–Zel'dovich effect (see Section 2.6) makes a distinctive change in the spectrum of the CMBR. This predicted change in the spectrum has not been observed and this is the major reason why the bremsstrahlung model is rejected in Big-Bang cosmology.

2.2.2 X-rays in CC

In CC, the basic component of the universe is plasma with a very high temperature, and with low enough density to avoid the Sunyaev–Zel'dovich effect (Section 2.6). The background X-ray emission is produced in this plasma by the process of free-free emission (bremsstrahlung). The observations of the background X-ray emission are analyzed in order to measure the density and temperature of the plasma. In CC, this density is the major free parameter and it determines the size of the universe and the value of the Hubble constant. In addition, the temperature of the plasma determined from the X-ray measurements can be compared with the predicted value from CC of $2.56 \times 10^9\,\mathrm{K}$ (Part 3).

The first step is to calculate the expected X-ray emission from high temperature plasma in thermal equilibrium. Here the dominant mechanism is bremsstrahlung radiation from electron-ion and electron-electron collisions. With a temperature T and emission into the frequency range ν to $\nu + d\nu$ the volume emissivity per steradian can be written as

$$\begin{aligned} j_\nu(\nu)d\nu &= \left(\frac{16}{3}\right)\left(\frac{\pi}{6}\right)^{1/2} r_0^3 m_e c^2 \left(\frac{m_e c^2}{kT}\right)^{1/2} \\ &\quad \times g(\nu,T)\exp\left(-\frac{h\nu}{kT}\right) N_e \sum Z_i^2 N_i \, d\nu, \end{aligned} \tag{1}$$

where $g(\nu, T)$ is the Gaunt factor, N_e is the electron number density, N_i is the ion number density and r_0 is the classical electron radius and the other symbols have their usual significance (Nozawa, Itoh & Kohyama, 1998). In SI $j_\nu(\nu)$ has the units of $\mathrm{W\,m^{-3}\,Hz^{-1}}$. As it stands this equation does not include the electron-electron contribution. Nozawa et al. (1998) and Itoh et al. (2000) have done accurate calculations for many light elements. Based on

Table 1: List of background X-ray data used.

Name	Instrument	Reference
Gruber	HEAO 1 A-4	Gruber et al. (1999)
Kinzer	HEAO 1 MED	Kinzer et al. (1997)
Dennis	OSO-5	Dennis et al. (1973)
Mazets	Kosmos 541	Mazets et al. (1975)
Mandrou	Balloon	Mandrou et al. (1979)
Trombka	Apollo 16, 17	Trombka et al. (1977)
Horstman	Rocket	Horstman-Morr. et al. (1974)
Fukada	Rocket	Fukada et al. (1975)

their calculations Professor Naoki Itoh (http://www.ph.sophia.ac.jp/) provides a subroutine to calculate the Gaunt factor that is accurate for temperatures greater than 3×10^8 K. It is used here. Let the average density be expressed as the number of hydrogen atoms per unit volume ($N = \rho/M_H$ m^{-3}). Then it is convenient to define $n_e = N_e/N$ and

$$n_i = \sum N_i Z_i^2 / N.$$

where the sum is over all species present. Because of the very high temperature, we can assume that all atoms are completely ionized. Thus, Eq. 1 including the Gaunt factor provides the production rate of X-ray photons as a function of the plasma temperature and density. The next step is to compute the expected intensity at an X-ray detector. Consider an X-ray photon that is produced at a distance $R\chi$ from the detector. During its travel to the detector, it will have many curvature-redshift interactions. Although the photon is destroyed

in each interaction, there is a secondary photon produced that has the same direction but with a slightly reduced energy. It is convenient to consider this sequence of photons as a single particle and to refer to it as a primary photon. The important result is that the number of these primary photons is conserved. Therefore, we need the production distribution of the number of photons per unit energy interval. The number of photons emitted per unit volume per unit time in the energy interval ε to $\varepsilon + d\varepsilon$ is given by

$$j_n(\varepsilon)\, d\varepsilon = \frac{j_\nu(\nu)}{\varepsilon} h\, d\nu, \tag{2}$$

where $\varepsilon = h\nu$, h is Plank's constant and $j_\nu(\nu)$ is the energy distribution per unit frequency interval. Now consider the contribution to the number of X-rays observed by a detector with unit area. Because the universe is static, the area at a distance R from the source is the same as the area at a distance R from the detector. Since there is conservation of these photons, the number coming from a shell at radius R per unit time and per steradian within the energy interval ε to $\varepsilon + d\varepsilon$ is

$$\frac{dn(r)}{dt}\, d\varepsilon = j_n(\varepsilon) d\varepsilon R\, d\chi.$$

Next, we integrate the photon rate per unit area and per steradian from each shell where the emission energy is ε and the received energy is ε_0 to get

$$I_n(\varepsilon_0)\, d\varepsilon_0 = R \int_0^{\chi_m} j_n(\varepsilon)\, d\varepsilon\, d\chi,$$

where $\varepsilon = (1 + z)\varepsilon_0$ and it is assumed that the flux is uniform over the 4π steradians. Furthermore, it is useful to change the independent coordinate to the redshift parameter z. Then using Eq. 2 we get

$$I_\nu(\nu_0)\, d\nu_0 = \frac{c}{H} \int_0^{z_m} \frac{j_\nu(\nu)}{1+z}\, dz\, d\nu_0,$$

where H is the Hubble constant and the change in bandwidth factor $d\nu/d\nu_o$, cancels the $(1+z)$ factor that comes from the change in variable from $d\chi$ to dz but there is another divisor of $(1+z)$ that accounts for the energy lost by each photon. Thus the energy flux per unit area, per unit energy interval, per unit frequency and per solid angle is given by Eq. 3 where Plank's constant is included to change the differential from frequency to energy. The z_m limit of 8.2 comes from the limit of $\chi \leqslant \pi$.

$$\begin{aligned} I_\nu(\nu_0) &= \left(\frac{16}{3}\right)\left(\frac{\pi}{6}\right)^{1/2} \frac{r_0^3 m_e c^3}{h} \left(8\pi G M_H\right)^{-1/2} \left(\frac{mc^2}{kT}\right)^{1/2} \\ &\quad \times n_e n_i N^{3/2} \int_0^{z_m} \frac{g\left((1+z)\nu_0, T\right)}{(1+z)} \exp\left(-\frac{h(1+z)\nu_0}{kT}\right) dz \\ &= \frac{1.9094 \times 10^3 \,\mathrm{keV}}{\mathrm{keV\,m^2\,s\,sr}} \left(\frac{mc^2}{kT}\right)^{1/2} n_e n_i N^{3/2} \\ &\quad \times \varepsilon_0 \int_0^{z_m} \frac{g\left((1+z)\nu_0, T\right)}{(1+z)} \exp\left(-\frac{h(1+z)\nu_0}{kT}\right) dz. \end{aligned} \tag{3}$$

The density N is obtained by fitting Eq. 3 to the observed data as a function of the temperature T, and then extracting N from the normalization constant. The X-ray data used is tabulated in Table 1. It consists of the background X-ray data cited in the literature and assessed as being the latest or more accurate results. Preliminary analysis showed that there were some discrepant data points that are listed in Table 2 in order of exclusion.

Very hard X-rays cannot be produced even by this hot plasma and are presumably due to discrete sources (Holt, 1992). Since bremsstrahlung is very sensitive to the presence of heavy elements, results are presented for four different abundances of hydrogen, helium, and 'metals'. The 'metals', which is a descriptor for all the other elements, were simulated by an element with $< Z >$=8.4,

Table 2: Background X-ray data: rejected points.

Source	Energy	Flux density	χ^2
	keV	keV/(keV cm^2 s sr)	(1 DoF)
Gruber	98.8	0.230±0.012	108.6
Gruber	119.6	0.216±0.022	65.2
Fukada	110.5	0.219±0.011	66.6
Gruber	152.6	0.140±0.022	50.9
Fukada	179.8	0.110±0.005	41.5
Gruber	63.9	0.484±0.034	25.1

Table 3: Abundances for four models.

Model	%H	%He	%metals	N_e/N	$\sum N_i Z_i^2/N$
A	100.0	0.0	0.0	1.000	1.000
B	92.17	8.5	0.0	0.875	1.002
C	92.06	7.82	0.12	0.868	1.061
D	91.91	7.82	0.28	0.860	1.135

$< Z^2 >$=75.3 and $< A >$=17.25.

These values were derived from the abundances given by Allen (1976). The details of the four different abundances are shown in Table 3 where the percentages are by number and the last two columns show the relative number of electrons and average value of Z^2 per unit hydrogen mass. Thus the models are A: pure hydrogen, B: hydrogen with 8.5% helium, C: normal abundance and D: similar to C but with enhanced 'metals'.

The results of the fit of the data to these models is given in Table 4 where

Table 4: Fitted parameters for four abundance models.

Model	N	$T_9{}^a$	χ^{2b}	$N_e{}^c$
A	1.93±0.02	2.62±0.04	167.4	1.93
B	1.55±0.01	2.62±0.04	167.6	1.35
C	1.16±0.01	2.61±0.04	168.5	1.01
D	0.88±0.01	2.61±0.04	169.0	0.75

[a]Temperature in units of 10^9K

[b]all for 74 DoF

[c]the electron number density (m^{-3})

the errors are the fitted uncertainties (1σ). Fig. 6 shows the flux density for the fitted curve for model B and for the observations as a function of energy.

Most of the X-ray flux below 10 keV and part of the flux just above 10 keV is emission from discrete sources. The deviation from the curve at energies above about 300 keV arises from X-rays coming from discrete sources. In the intermediate region where bremsstrahlung should dominate, there are clear signs of some minor systematic errors. In addition, there appears to be some variation between the data sets. It is not clear whether the discrepancy between the observed points and the predicted flux densities is due to an inadequate theory, inadequate X-ray emission model, or systematic errors in the observations. After all the measurements are very difficult and come from a wide range of rocket, ballon and satellite experiments. In particular, the recent HEAO results Kinzer et al. (1997) differ from earlier results reported by Marshall et al. (1980).

It is apparent from Table 4 that although the measured temperature is rel-

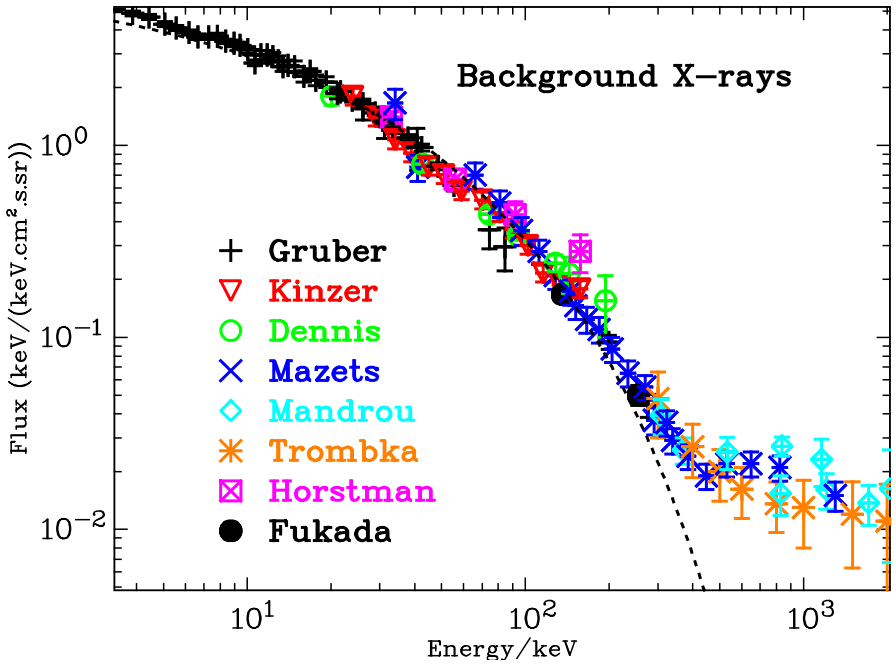

Figure 1: Background X-ray spectrum. See Table 1 for list of observations. The dashed (black) line is best fit from 10 keV to 300 keV.

atively insensitive to the assumed abundance the density estimate is strongly dependent. This is because bremsstrahlung depends mainly on the number and to a lesser extent the type of charged particles whereas the density also depends on the number of neutrons in each nucleus.

The power law fit parameters are the same for all the models and are shown in Table 5 for model B. This model was chosen because it uses the standard abundances that might be expected in the plasma and it has a relatively good fit to the observations. The quoted errors are the formal uncertainties of the fit. There are certainly larger, unknown systematic errors.

For the measured density of $N = 1.55 \pm 0.01\,\mathrm{m}^{-3}$ the calculated value of the Hubble constant is $H = 64.4 \pm 0.2\,\mathrm{km\,s}^{-1}\,\mathrm{Mpc}^{-1}$ (c.f. Part 3: Eq. 28). Further

Table 5: Fitted parameters for model B.

Quantity	Symbol	Value
Mean density	N	$1.55 \pm 0.01\,\mathrm{m}^{-3}$
Electron density	N_e	$1.35 \pm 0.01\,\mathrm{m}^{-3}$
Electron temperature	T_e	$(2.62 \pm 0.04) \times 10^9\,\mathrm{K}$
Power law value at 1 Mev	a	0.019 ± 0.001
Exponent	b	-0.49 ± 0.19

properties of the universe based on this density are shown in Part 3: Table 3. That said, this bremsstrahlung model for the background X-ray emission within CC provides a good fit to the relevant observations. A crucial test of CC is that it predicts a temperature of 2.56×10^9 K for the cosmic plasma. The temperature estimated from fitting the X-ray data is $(2.62 \pm 0.04) \times 10^9$ K. There is remarkable agreement between these values. It should be emphasized that the predicted temperature is a pure prediction from the theory without any dependence on observations. This agreement and the good fit to the observations gives strong support to CC.

In CC the argument against bremsstrahlung based on the Sunyaev–Zel'dovich effect is not valid because the density of the gas is much less and the CMBR has a different source. It has been shown that the X-ray data in the range from about 10 Kev to about 300 kev can be explained by bremsstrahlung from the cosmic gas. The fitted temperature was $2.62 \pm 0.04 \times 10^9$ K and the fitted density was $N = 1.55 \pm 0.01$ hydrogen atoms per cubic meter ($2.57 \times 10^{-27}\,\mathrm{kg\,m}^{-3}$).

At present BB does not have a good explanation for background X-ray radiation in the intermediate range of energies. Curvature cosmology can com-

pletely explain these observations as coming from bremsstrahlung in a hot cosmic plasma.

2.3 Cosmic microwave background radiation

The cosmic microwave background radiation (CMBR) is one of the major success stories for BB. The observed radiation has a spectrum that is extremely (by normal cosmological standards) close to a black body spectrum which means that it can be described by a single parameter, its temperature. Observations of the CMBR spectrum were obtained from the FIRAS instrument on the *Cobe* satellite by Mather et al. (1990). They measured the temperature of the CMBR to be 2.725 K. This temperature is in agreement with the observations of Roth & Meyer (1995) who measured a temperature of $2.729(+0.023, -0.031)$ K using cyanogen excitation in diffuse interstellar clouds. It must be remembered that there is nothing special about a black body spectrum. If the radiation is quantized and all energy levels are freely available the black body (Plank function) is the thermal equilibrium spectrum. It is the maximum entropy solution. The black body is only required to permit the number of photons in each energy level come into equilibrium. Thus in a general sense the black body spectrum is the default spectrum.

2.3.1 CMBR in BB

In BB the CMBR is the relic radiation that has been redshifted from the high temperature radiation that was in equilibrium with matter at the time when the ions combined with electrons to produce neutral atoms which are transparent. This decoupling of the radiation from matter occurred at a redshift of about

$z = 1000$. The exact temperature of the subsequent CMBR depends on the baryonic density parameter. Over time the redshift of the photons results in a decrease of their energy corresponding to an identical decrease in temperature without changing the shape of the spectrum. Thus BB predicts a black body spectrum with only a poor estimate of its temperature.

2.3.2 CMBR in CC

In CC, the CMBR comes from the curvature-redshift process acting on the high-energy electrons and ions in the cosmic plasma. Examination of Part 3: Eq. 11 shows that even for very high temperature plasma the emission from electrons will dominate that from other ions. The energy loss occurs when an electron that has been excited by the passage through curved spacetime interacts with a photon or charged particle and loses its excitation energy. Ideally, the theoretical model would provide the number distribution of secondary photons as a function of their energy. This distribution would then be combined with the distribution of electron energies to obtain the production spectrum of low-energy secondary photons from the plasma. The final step would be to integrate this production spectrum over all distances allowing for the geometry and curvature redshift. The result would be the spectrum of photons that would be observed at any point in space.

We assume that the production spectrum for the photons is peaked at much larger energies than the cosmic microwave background photons. Then the cosmic microwave photons are seen to have had many curvature-redshift interactions. At each of these interactions the photons lose a small fraction of energy to very low energy photons that have frequencies less than the plasma frequency.

Thus these low energy secondaries only exist as evanescent waves with their energy heating the plasma. Now since the radiation field is quantized the choice of the precise frequency of the large secondary photon is controlled by the number of available modes of oscillation. Being evanescent the very low energy photons are not relevant and the number of modes of oscillation is determined by the wavelength of the large secondary photon. Thus although the average energy loss rate is determined by the average density the selection of the number and occurrence of individual interactions depends on the quantization of the radiation field. All modes are available and in equilibrium the rate of photons entering a mode will equal the rate of photons leaving a mode. Because of the very large number of curvature-redshift interactions that have occurred since the original photon was produced the distribution of number of photons in each mode is essentially determined by the curvature-redshift interactions and not by the original spectrum. Thus the observed spectrum will be the maximum entropy spectrum determined by the allowed modes of the radiation field. In equilibrium there is a constant energy density for these photons and as originally shown by Einstein (Longair, 1991) the maximum entropy solution is that for a black body with a well defined temperature. The assumption of equilibrium enables us to equate the energy loss by the electrons to the energy loss by the CMBR photons and then to use Stefan's law to determine the temperature of the CMBR.

This brings up the problem of how the excited electrons produce the CMBR photons. Since conservation of energy and momentum prevents an excited free electron from emitting a photon, there must be an interaction with a third particle. A quick calculation shows that Thompson (Compton) scattering with the

existing CMBR photons is too infrequent. The only other suitable interaction is Rutherford scattering off other electrons and ions. Since its last gravitational interaction, the electron will have become excited and have an excess of energy due to its passage through curved spacetime. At the Rutherford scattering this excitation energy is transferred to secondary photons which become the CMBR after many curvature-redshift interactions.

The balance between the energy loss by the X-ray electrons and the energy loss by the CMBR photons implies that there is an overall conservation of energy with the photon energy loss being returned to the electrons. Since the secondary photons produced by curvature-redshift interaction of the CMBR photons have frequencies well below the plasma frequency (of about 10 Hz), their energy must go into plasma waves which are dissipated with their energy going to heat the plasma. These processes are not driven by temperature differences so that there is no change in entropy.

For equilibrium, the energy gained by these secondary photons must equal the energy lost by the electrons. Since the dominant energy loss by photons in the cosmic space is via curvature redshift, we can equate the two loss rates to determine the average energy of these photons. For electrons, or indeed any non-zero rest mass particle, the energy loss rate is given by Part 3: Eq. 11. Thus the energy loss rate for an electron is

$$\frac{d\varepsilon}{dt} = H\left[\beta^3(\gamma^2 - \frac{1}{2})^{1/2}(\gamma - 1)\right] m_e c^2, \tag{4}$$

where to prevent confusion with the symbol for temperature the electron's kinetic energy is denoted by $\varepsilon = (\gamma - 1)m_e c^2$ and the an extra factor of β comes from conversion of distance rate to time rate. The next step is to average this energy loss over the distribution of electron energies. Since the electrons are

relativistic, the appropriate distribution is Jüttner distribution, which is (de Groot, Leeuwen & van Weert, 1980)

$$n(p)d^3p = \frac{d^3p}{h^3} \exp\left(-\frac{\gamma mc}{kT_e}\right). \tag{5}$$

With a change of variable to γ it becomes

$$n(\gamma)\, d\gamma \propto \gamma(\gamma^2 - 1)^{1/2} \exp\left(-\frac{\gamma m_e c^2}{kT_e}\right) d\gamma. \tag{6}$$

Then integrating Eq. 4 over all the electron energies we get

$$\overline{\frac{d\varepsilon}{dt}} = HN_e m_e c^2 f(T_e), \tag{7}$$

where N_e is the density of the electrons and $f(T_e)$ is average of the γ terms. Where we have

$$f(T_e) = \frac{\int_1^\infty \left[\left(\gamma^2 - \frac{1}{2}\right)^{1/2} \beta^3(\gamma - 1)\right] n(\gamma)\, d\gamma}{\int_1^\infty n(\gamma)\, d\gamma}. \tag{8}$$

Although the Jüttner distribution can be integrated analytically in terms of modified Bessel functions, it is just as easy to evaluate both integrals numerically. Table 6 shows some values for the function $f(T_e)$ as a function of the electron temperature T_e.

Consider the CMBR photons at one point in space. All of these photons will have been produced in one of the shells surrounding that point. In a static cosmology the contribution from each shell depends only on the thickness of the shell and is independent of the radius of the shell. However in CC there is an energy loss due to curvature redshift which means that the average energy that comes from a shell at redshift z is reduced by the factor $(1 + z)^{-1}$. Thus the average energy at the select point is less than the average energy of production by the integration of this factor with respect to distance. By using Part 3:

Table 6: Some values for function $f(T)$.

$T_e/10^9$	$f(T_e)$	$T_e/10^9$	$f(T_e)$	$T_e/10^9$	$f(T_e)$
1.2	0.138	1.8	0.443	2.4	0.967
1.3	0.175	1.9	0.515	2.5	1.076
1.4	0.217	2.0	0.592	2.6	1.193
1.5	0.265	2.1	0.676	2.7	1.316
1.6	0.318	2.2	0.767	2.8	1.445
1.7	0.378	2.3	0.863	2.9	1.582

Eq. 30 to convert from distance to redshift the ratio is

$$\frac{1}{\sqrt{3}}\int_0^\infty \frac{1}{(1+z)^2}dz = \frac{1}{\sqrt{3}}. \tag{9}$$

Thus the electron energy loss rate must be $\sqrt{3}$ times larger than the energy loss rate by the CMBR photons. This is because the CMBR photons have already lost a major part of their energy since production during which time their spectrum is transformed in that for a black body.

The next step is to calculate the energy loss rate for the CMBR photons. If the CMBR photons are the result of curvature redshift acting on the cosmic electrons and the system is in equilibrium these two loss rates should be equal. For a black body spectrum then the energy density of the CMBR photons near us must be the same as that for a uniform black body radiation with the same temperature. However, because the universe is homogeneous, the energy density must be the same everywhere. Then using Eq. 7 and Stefan's equation we get

$$\begin{aligned} \frac{4\sigma}{c}T_p^4 H &= \frac{N_e m_e c^2}{\sqrt{3}} f(T_e) H, \text{ hence} \\ T_p^4 &= 62.4786 N_e f(T_e). \end{aligned}$$

where σ is the Stefan-Boltzmann constant and, not surprisingly, the Hubble constant cancels. Then from Table 6 we get $N_e = 1.35$ and for a temperature of $(2.62 \pm 0.04) \times 10^9$ K the calculated value of the function $f(T_e)$ is 1.215. These numbers result in a predicted temperature for the CMBR of 3.18 K. Probably the largest error in these temperature estimates comes from the uncertainty in the nuclear abundances. For the four abundance models (section 2.2) the predicted temperatures of the CMBR are 3.48 K, 3.18 K, 2.95 K and 2.74 K for the models 1, 2, 3 and 4 respectively. The main dependence is due to the differences in the electron density. Another important factor is the assumption that the universe has uniform density when it is apparent that it has large density variations.

2.3.3 CMBR conclusions

Both cosmologies offer argument to support the black body spectrum. Those for BB are well founded those for CC are less well founded. Against that BB does not have a good prediction for the temperature while CC predicts a narrow range of temperatures that is in excellent agreement with the observed temperature.

2.4 CMBR at large redshifts

The temperature of the CMBR has been measured at large redshifts using two different methods. The first method measures the column density ratio of the fine structure absorption lines originating from the fundamental and first excited states of carbon (Ge et al., 1997; Lima, Silva & Viegas, 2000; Srianand, Petitjean & Ledoux, 2000; Srianand et al., 2008). These lines are seen in the Lyman-α forest that is observed in the spectra from a bright quasar. The tem-

perature estimate is based on the relative strengths of these spectral lines. For these measurements to be valid, it is essential that the line widths and column densities are well understood. In CC the width of a spectral line is increased by the differential redshift as the photons traverse the absorbing gas. This change in the widths of spectral lines makes the very complex interpretation of the spectra required to estimate the temperature of the radiation suspect. Thus, until this interpretation is fully understood in the context of CC, CMBR temperature results from this method cannot be trusted.

The second method uses the Sunyaev–Zel'dovich effect acting on the CMBR by the gas in clusters of galaxies Battistelli et al. (2002). By using multiple frequencies, it is possible to minimize the effects due to properties of the clusters on the result. However the method is flawed in CC because the CMBR has a different cause from that in Big-Bang cosmology. Thus, these results cannot be taken as showing a dependence of the temperature of the CMBR on redshift until the complete mechanism is understood in the context of CC.

2.5 Fluctuations in the CMBR

One of the arguments for the interpretation of the CMBR in BB is that there are extensive models that can explain the density and polarization of spatial fluctuations in the observed radiation. In the model proposed for curvature radiation these fluctuations will also occur but in this case they are due to variations in the density of the cosmic plasma. The CMBR seen through the denser gas within a galactic cluster will have lower than average temperature. Cabre et al. (2006) show some support for this model in that they have correlated data from the Wilkinson Microwave Anisotropy Probe (WMAP) with galaxy

samples from the SDSS DR4 galaxy survey and found a significant correlation for the intensity fluctuations with galaxy density.

2.6 Dark matter

The theoretical problems with dark matter have already been canvassed. Here we concentrate on the observational evidence. All observational evidence for dark matter comes from the application of Newtonian gravitational physics to either clusters of objects or the rotation of galaxies. Galaxy rotation will be dealt with in Section 2.12. The original concept for dark matter comes from applying the virial theorem to the Coma cluster of galaxies (Zwicky, 1937). The virial theorem (Goldstein, 1980) is a statistical theorem that states that for an inverse square law the average kinetic energy of a bound system is equal to half the potential energy (i.e. $2T + V = 0$). Then with knowing the linear size of the cluster and measuring the mean square spread of velocities we can estimate the total mass of the cluster. There is no doubt that applying the virial theorem to the Coma and other clusters of galaxies provides mass estimates that can be several hundred times the mass expected from the total luminosity. Even the mass of inter-galactic gas is not enough to overcome this imbalance. In BB cosmology dark matter has been introduced to make up for the shortfall of mass.

However if CC is valid then it is possible that the observed redshifts are not due to kinematic velocities but are curvature redshifts produced by the inter-galactic gas. The purpose of this section is to show that curvature redshift can explain the galactic velocities without requiring dark matter. For simplicity, we will use the Coma cluster as a test bed. Not only is it very well studied, but it also has a high degree of symmetry and the presence of an inter-galactic gas

cloud is known from X-ray observations. Watt et al. (1992) and Hughes (1989) have fitted the density of the gas cloud to an isothermal-model with the form

$$\rho = \rho_0 \left(1 + \left(\frac{r}{r_e}\right)\right)^{-\alpha}, \tag{10}$$

with a center at $12^h59^m10^s$, $27^\circ59'56''$ (J2000) and with $r_e = 8.8' \pm 0.7'$, $\alpha = 1.37 \pm 0.09$, $\rho_0 = (2.67 \pm 0.22) \times 10^3 h_{50}^2\,\mathrm{m}_H\,\mathrm{m}^{-3}$. The central density is obtained from the X-ray luminosity and has a strong dependence on the distance. Watt et al. (1992) assumed a Hubble constant of 50 $\mathrm{km\,s^{-1}\,Mpc^{-1}}$. With a mean velocity of 6,853 $\mathrm{km\,s^{-1}}$ (Colless & Dunn, 1996) and with this Hubble constant, the distance to the Coma cluster is 137 Mpc. Recently Rood (1988) using the Tully–Fisher relation to measure the distance modulus to the galaxies in the Coma cluster, to observe a value of 34.4±0.2 mag whereas Liu & Graham (2001) using infrared surface brightness fluctuations get 34.99±0.21 mag. The average is 34.7 mag that corresponds to a distance of 87.1 Mpc. This is consistent with the distance of 85.6 Mpc given by Freedman et al. (2001). Thus putting $h = 0.7$ gives a corrected central gas density of $\rho_0 = (6.61 \pm 0.54) \times 10^{-3}\,\mathrm{m}_H\,\mathrm{m}^{-3}$.

The galactic velocity data are taken from Beijersbergen & van der Hulst (2004) who provide information for 583 galaxies. The velocity centroid of the Coma cluster is $12^h59^m19^s$, $27^\circ52'2''$ (J2000). They find that early-type galaxies (E+S0+E/S0) have a mean velocity of 9,926 $\mathrm{km\,s^{-1}}$ and a rms (root-mean-square) velocity, dispersion velocity, of 893 $\mathrm{km\,s^{-1}}$. Let us assume that all the galactic velocities are due to curvature redshift. That is we assume that the actual velocities, the peculiar velocities, are negligible. Then the redshifts for the galaxies are calculated (in velocity units) by

$$v = v_0 + \int_0^Z 51.691 \sqrt{N\,(Z)}\,dZ\,\mathrm{km\,s^{-1}}, \tag{11}$$

Table 7: Coma velocity dispersions for some distances.

Distance/Mpc	50	87	100	150
Dispersion /km s^{-1}	318	554	636	955

where Z is the distance from the central plane of the Coma cluster to the galaxy measured in Mpc, $N(Z)$ is the density of the inter-galactic gas cloud and v_0 is the average velocity of the galaxies in the cluster. The problem here is that we do not know Z distances. Nevertheless, we can still get a good estimate by assuming that the distribution in Z is statistically identical to that in X and in Y. In a Monte Carlo simulation, each galaxy was given a Z distance that was the same as the X (or Y) distance of one of the other galaxies in the sample chosen at random. For 50 trials, the computed dispersion was 554 km s^{-1} which can be compared with the measured dispersion of 893 km s^{-1}. Curvature cosmology has predicted the observed dispersion of galactic velocities in the Coma cluster to within a factor of two. Considering that this is a prediction of the cosmological model without fitting any parameters and ignoring all the complications of the structure both in the gas and galactic distributions the agreement is remarkable.

Since the distance to the Coma cluster is an important variable, the computed velocity dispersion from the Monte Carlo simulation for some different distances (all the other parameters are the same) is shown in Table 7. Thus, the redshift dispersion (in velocity units) is approximately a linear function of the Coma distance. This is not surprising since in this context the distance is mainly a scale factor.

Beijersbergen & van der Hulst (2004) note that a better fit to the velocity

distribution is provided by the sum of two Gaussian curves. Their best fit parameters for these two Gaussians are $v_1 = 7,501 \pm 187\,\mathrm{km\,s^{-1}}$, with $\sigma_1 = 650 \pm 216\,\mathrm{km\,s^{-1}}$ and $v_2 = 6641 \pm 470\,\mathrm{km\,s^{-1}}$, with $\sigma_2 = 1,004 \pm 120\,\mathrm{km\,s^{-1}}$. This double structure is supported by Colless & Dunn (1996) who argue for an ongoing merger between two sub clusters centered in projection on the dominant galaxies NGC 4874 and NGC 4889. In addition, Briel Henry, & Bhringer (1992) found evidence for substructure in the X-ray emission and Finoguenov et al. (2004) and White, Briel & Henry (1993) have measured the X-ray luminosity of individual galaxies in the Coma cluster showing that the model for the gas used above is too simple. The net effect of this substructure is that the observed velocity dispersion would be different from that predicted by a simple symmetric model. Thus, it appears that substructure makes it very difficult to achieve a more accurate test of CC using the Coma cluster.

There is an important difference between curvature redshift and models that assume that the redshifts of the galaxies within a cluster are due to their velocities. Since the laws of celestial mechanics are symmetric in time, any galaxy could equally likely be going in the opposite direction. Thus a galaxy with a high relative (Z) velocity could be in the near side of the cluster or equally likely on the far side of the cluster. However, if the redshifts are determined by curvature redshift then there will be a strong correlation in that the higher redshifts will come from galaxies on the far side of the cluster. A possible test is to see if the apparent magnitudes are a function of relative redshift. With a distance of 87.1 Mpc the required change in magnitude is about 0.025 $\mathrm{mag\,Mpc^{-1}}$. A simple regression between magnitude of Coma galaxies (each relative to its type average) and velocity did not show any significant dependence. Although this

was disappointing, several factors can explain the null result. The first is the presence of substructure; the second is that the magnitudes for a given galactic type have a standard deviation of about one magnitude, which in itself is sufficient to wash out the predicted effect; and thirdly mistyping will produce erroneous magnitudes due to the different average velocities of different types. In support of the second factor we note that for 335 galaxies with known types and magnitudes, the standard deviation of the magnitude is 1.08 mag and if we assume that the variance of the Z distribution is equal to the average of the variances for the X and Y distributions then the expected standard deviation of the slope is 0.076 mag Mpc^{-1}. Clearly, this is such larger than the expected result of 0.025 mag Mpc^{-1}. It is expected that better measurements or new techniques of measuring differential distances will in the future make this a very important cosmological test.

In BB observations of the velocity dispersion of clusters of galaxies cannot be explained without invoking an ad hoc premise such as dark matter. However CC not only explains the observations but also makes a good prediction, without any free parameters, of its numerical value.

2.7 The Sunyaev–Zel'dovich effect

The Sunyaev–Zel'dovich effect (Sunyaev & Zel'dovich, 1970; Peebles, 1993) is the effect of Thompson scattering of background radiation by free electrons in the intervening medium. The technique depends on knowing the spectrum of the background source and then measuring the changes in the spectrum due to the intervening plasma. In particular, it is the scattering in both angle and frequency of the cosmic microwave background radiation (CMBR) by electrons

in the cosmic plasma. Because of the rapidly increasing density (like $(1+z)^3$) with redshift this is an important effect in BB.

The effect is often characterized by the dimensionless Compton y-parameter, which for a distance x through non-relativistic thermal plasma with an electron density of N_e has the value

$$y = \frac{kT_e}{m_e c^2}\sigma_T N_e x = 3.46 \times 10^{-16} N_e T_e x \,\mathrm{Mpc}, \tag{12}$$

where σ_T is the Thompson cross-section. An object at redshift z is at the distance $x = R\chi = 5.80 \times 10^3 N_e^{1/2} \log(1+z)\,\mathrm{Mpc}$. Hence, using $T_e = 2.62 \times 10^9\,\mathrm{K}$, $N_e = 1.35\,\mathrm{m}^{-3}$ we get $y = 9.2 \times 10^{-6}\log(1+z)$.

Using the CMBR as a source the Sunyaev–Zel'dovich effect has been observed and Mather et al. (1990) report an observed upper limit of $y = 0.001$, and more recently Fixsen et al. (1996) report $y = 1.5 \times 10^{-5}$. Using this limit with Eq. 12 shows that there is no effect in CC if $z < 4.1$. Although in CC the CMBR has a more local origin it is of interest to note that this analysis assumes that each photon has many Compton interactions. For this electron density the Compton mean free path is 575 Gpc whereas the distance to $z = 4.1$ is about 3.7 Gpc which means that a negligible number of the photons will have an interaction with the high temperature electrons. Furthermore the photon energy distribution for a single interaction has a different spectrum for that for the normal Sunyaev–Zel'dovich effect (Longair, 1991; Sunyaev, 1980). Bielby & Shanks (2007) extend the results of Lieu, Mittaz & Zhang (2006) to show that not only was the Sunyaev–Zel'dovich effect less than what was expected but that it tendered to disappear as the redshift went from 0.1 to 0.3. The conclusion is that CC is completely consistent with the experimental observations of the Sunyaev–Zel'dovich effect on the CMBR. The conclusion is that although

the Sunyaev–Zel'dovich effect is important in BB it is not important in CC.

2.8 Gravitational lensing

There are more than 50 known gravitational lens where a quasar or distant galaxy has one or more images produced by a nearer lensing galaxy or cluster of galaxies. A set of these lensing systems has been examined in the context of CC to see if it offers a consistent and possibly simpler explanation. The two important measures are the prediction of the mass of the lensing galaxy and the determination of the Hubble constant from the time delays between variations in the luminosity of different images. Since the delay measurement is easily done all that is needed is to measure the different path lengths. This path difference involves both geometric and general relativistic corrections.

One of the remarkable properties of gravitational lenses is that the geometry is completely determined by a two-dimensional lensing potential which can be expressed in terms off a surface density at the position of the lensing galaxy. For thin lenses, any two systems with the same surface density have the same lens effect. Now the usual way to determine the surface density is to measure the widths of spectral lines, assume that the width is due to velocity and then use the virial theorem to obtain the surface density. However in CC the widths of spectral lines are likely to have a large component due to the effects of curvature redshift from dust and gas in the lensing object. Thus the widths are not a reliable measure of area density and this method cannot be used. Instead some double image gravitational lens were investigated using a very simple point sources lens in order to see if the observations could be consistent with CC. However because of the paucity of examples and the wide range of characteristics

there was no test that showed a significant difference between BB and CC. The data was consistent with both cosmologies. Currently the modeling and the data are not sufficient to choose between the cosmologies. However a more thorough analysis within the paradigm of CC may be more definite.

2.9 Lyman-α forest

The Lyman-α (Lyα) forest is the large number of absorption lines seen in the spectra of quasars. Most of the lines are due to absorption by clouds of neutral hydrogen in the line of sight to the quasar. Some of the lines are due to other elements or due to Lyman-β absorption. Because of the redshift between the absorbing cloud and us, the lines are spread out over a range of wavelengths. Usually the analysis is confined to lines between the Lyα (at a wavelength of 121.6 nm) and Lyβ (at 102.5 nm). Thus, each quasar provides a relatively narrow spectrum of Ly-α lines at a redshift just less than that for the quasar. Since the advent of spacecraft telescopes, in which can observe the ultraviolet lines, and by using many quasars the complete redshift range up to the most distant quasar has been covered. The large redshift range makes the Lyman α spectra potentially a powerful cosmological tool.

The obvious cosmological observation is the density of lines as a function of redshift but as discussed by Rauch (1998) in an excellent review, there are many important observational problems. The first, which has now been overcome, is that the spectra must have sufficient resolution to resolve every line. The second is that most lines are very weak and the number of resolved lines can depend greatly on the signal to noise ratio. This is accentuated because the steep spectrum for the density of lines as a function of their strength means that

a small decrease in the acceptance level can drastically increase the number of observed lines. The third problem is that each quasar only provides a set of lines in a narrow range of redshift and there are considerable difficulties in getting uniform cross-calibrations. In addition to these problems, it will be shown that curvature redshift can have a profound effect on the interpretation of the line widths and column densities.

Since in CC the distribution of clouds is independent of time or distance the expected density of lines as a function of redshift is

$$\frac{dn}{dz} = \frac{AcN_0}{H(1+z)}, \tag{13}$$

where N_0 is the volume density and A is the average area of a cloud. Most observers have fitted a power law with the form $(1+z)^\gamma$ to the observed line densities with a wide range of results. They vary from $\gamma = 1.89$ to $\gamma = 5.5$ (Rauch, 1998). All of which are inconsistent with the CC prediction of $\gamma = -1$. In CC there is the additional effect that much of the line broadening may be due to curvature redshift. Curvature redshift will be operating within the clouds so that the observed line width will be a combination of the usual Voigt profile and the change in the effective central frequency as the photons pass through the cloud. If the cloud has a density $\rho(x)$ at the point x, measured along the photon trajectory then the change in frequency from the entering frequency due to curvature redshift is

$$\frac{\Delta\nu}{\nu} = \frac{1}{c}\int \sqrt{8\pi G\rho(x)}dx.$$

In units of $N(x) = \rho(x)/m_H$ this is (with N in m^{-3} and dx in kpc)

$$\frac{\Delta\nu}{\nu} = -\frac{\Delta\lambda}{\lambda} = \int 1.724\times10^{-7}\sqrt{N(x)}dx.$$

Then the final profile will be the combination of the natural line width, the Doppler width due to temperature, any width due to bulk motions and the curvature redshift width. Now assuming pure hydrogen, the hydrogen column density is given by $N_H = \int N(x)dx$. Although it is unlikely that the line of sight goes through the center of the cloud, it is reasonable to expect a roughly symmetric distribution of gas with a shape similar to a Gaussian. We can define an effective density width by

$$x_w^2 = \int (x - \overline{x})^2 \, N(x)dx \, / \int N(x)dx.$$

Also define $N_0 = N_H/x_w$ and an effective velocity width $\Delta v = 51.68\eta x_w\sqrt{N_0}$ and where η is a small numeric constant that depends on the exact shape of the density distribution. Eliminating the central density, we get (with x_w in kpc)

$$\Delta v^2 = 8.656 \times 10^{-17}\eta^2 N_H x_w. \tag{14}$$

For values $N_H = 10^{19}\,\mathrm{m}^{-2}$, x_w=1 kpc and with η=1 we get Δv=29 $\mathrm{km\,s}^{-1}$. Since there is a wide variation in column densities and the effective widths are poorly known it is clear that curvature redshift could completely dominate many of the Lyman-α line widths and the others would require a convolution of the Doppler profile with the curvature redshift density effect. What is also apparent is that the very broad absorption lines may be due to curvature redshift acting in very dense clouds. Although there is uncertainty about the observed relationship between the line width and the column density, we note that for a fixed effective density width, Eq. 14 predicts a square relationship that may be compared with the exponent of 2.1 ± 0.3 found by Pettini et al. (1990). Clearly, there needs to be a complete re-evaluation of profile shapes, column-densities, and cloud statistics that allows for the effects of CC. We must await this analysis

to see whether the Lyman-α forest can provide a critical test of CC.

2.10 The Gunn–Peterson trough in high redshift quasars

The Gunn–Peterson trough is a feature of the spectra of quasars probably due to the presence of neutral hydrogen in the intergalactic medium. The trough is characterized by suppression of electromagnetic emission from the quasar at wavelengths less than that of the Lyman-α line at the redshift of the emitted light. This effect was originally predicted by Gunn & Peterson (1965). Although the Gunn–Peterson-trough has now been seen in several high redshift quasars Becker et al. (2001), Peng Oh & Furlanetto (2005), White et al. (2005) it is not seen in all quasars and appears to be strongly dependent on redshift. In BB the explanation is that it is only seen in very high redshift quasars where the intergalactic medium is still neutral but it is not seen in closer quasars because the medium has been re-ionized. In CC it has a more prosaic explanation.

We assume that the quasar is surrounded by a large halo or it lies within a cluster of galaxies which has, like many clusters, an internal gas cloud. The hypothesis is that the halo or gas cloud is cool enough to have a small but important density of neutral hydrogen that absorbs much of the quasar emission at shorter wavelengths than the Lyman-α emission. The important point is that as the radiation traverses the cloud it is redshifted by curvature redshift due to the density of the cloud. The Lyman-α radiation from the quasar is redshifted by the curvature redshift due to the density of the whole cloud. The absorption lines are only shifted by part of the cloud and appear at a shorter wavelength than the quasar Lyman-α emission. Consider the scattering probability of a photon with wavelength λ by the neutral hydrogen. The differential probability

is

$$dp = \pi c f_H r_0 f \int_{\nu_\alpha}^{\nu} N\,(r) g\,(\nu - \nu\alpha)\,dr,$$

where r_0 is the classical electron radius, f_H is the fraction of neutral hydrogen atoms, f is the oscillator strength (here $f = 0.416$), $N(r)$ is the gas density and g is the profile function that is strongly peaked about $\nu = \nu_\alpha$. At a distance r inside the cloud $\nu = \nu_q \exp(-ar)$ where ν_q) is its frequency at the beginning of the cloud and

$$a = \sqrt{\frac{8\pi G M_H n(r)}{c^2}} = 5.588 \times 10^{-27} \sqrt{n\,(r)}\,\mathrm{m}^{-1}.$$

A change of variable from r to ν and noting that the width of $g(\nu)$ is small compared to the value of ν_α and assuming a constant density $N = N(r)$ results in the approximation

$$p \approx \frac{\pi r_0 \lambda_\alpha f_H \sqrt{N}}{a} = 8.01 \times 10^4 f_H \sqrt{N}.$$

Clearly all the photons are scattered for quite low densities and a very small density of hydrogen atoms.

Having shown that total scattering is feasible the next step is to see why the effect is more pronounced for high redshift quasars. The basic equation for curvature redshift is $1 + z = \exp(cr/H)$ where r is the distance, H is the Hubble constant and $dz = a(1 + z)dr$. Thus the wavelength range that is observed over which the Gunn–Peterson effect is seen should scale as $(1 + z)$. Thus the probability of detection which depends on the wavelength range will be lower at smaller redshifts. Naturally the effect may not be seen or could be partially obscured depending on the individual characteristics of the cloud around each quasar.

Becker et al. (2001) report details of the quasar SDSS 1030+0524 which has an emission redshift of 6.29 and a Gunn–Peterson depression that has a width $dz = 0.21$. With this value we find that it can be explained by a cloud that has the constraint $N^{1/2}dr = 167$ where dr is in Mpc. With $dr = 2$ Mpc the required density is $7 \times 10^3\,\mathrm{m}^{-3}$ which is a feasible size and density for a large cluster cloud. Note that if the gas has high enough temperature f_H will be too small and no effect will be seen.

2.11 Nuclear abundances

One of the successes of BB is in its explanation of the primordial abundances of the light elements. Since the proposed CC is static, there must be another method of getting the 'primordial' abundances of light elements. In CC, the primordial abundance refers to the abundance in the cosmic gas from which the galaxies are formed. The first point to note is that in CC the predicted temperature of the cosmic gas is 2.56×10^9 K at which temperature nuclear reactions can proceed. The major difference with the production of helium and deuterium in the BB early universe is that the densities were incredibly higher in BB than they are in CC. It is postulated that in CC there is a continuous recycling of material from the cosmic gas to galaxies and stars and then back to the gas. Because of the high temperature, nuclear reactions will take place whereby the more complex nuclei are broken down to hydrogen, deuterium, and helium. Although this cycling can take many billions of years the very low density of the gas means that the cycle time may not be long enough for the nuclei densities to achieve statistical equilibrium. In addition, the major reactions required are the breaking down of heavier nuclei to lighter ones and

not those that construct nuclei. It is through the interactions of cosmic gas in CC that the light nuclei abundances are produced.

2.12 Galactic rotation curves

One of the most puzzling questions in astronomy is: why does the observed velocity of rotation in spiral galaxies not go to zero towards the edge of the galaxy. Simple Keplerian mechanics suggests that there should be a rapid rise to a maximum and then a decrease in velocity that is inversely proportional to the square root of the radius once nearly all the mass has been passed. Although the details vary between galaxies, the observations typically show a rapid rise and then an essentially constant tangential velocity as a function of radius out to distances where the velocity cannot be measured due to lack of material. The BB explanation is that this is due to the gravitational attraction of a halo of dark matter that extends well beyond the galaxy. We examine whether this rotation curve can be explained by curvature redshift.

Observations show that our own Galaxy and other spiral galaxies have a gas halo that is larger than the main concentration of stars. It is clear that if the observed redshifts are due to curvature redshift acting within this halo, the halo must be asymmetric; otherwise, it could not produce the asymmetric rotation curve. Now the observed velocities in the flat part of the curves are typically 100 to 200 $\mathrm{km\,s^{-1}}$. The first step is to see if curvature redshift provides the right magnitude for the velocity. For a gas with an average density of N_H the predicted redshift (in velocity units) is $5.17 \times 10^{-2} d\sqrt{N}\,\mathrm{km\,s^{-1}}$ where d is the distance in kpc. For realistic values of $d = 10\,\mathrm{kpc}$ and $N = 1.0 \times 10^5\ \mathrm{m^{-3}}$ the velocity is $163\,\mathrm{km\,s^{-1}}$. Thus, the magnitude is feasible. Although there could be

a natural asymmetry in a particular galaxy, the fact that the flattened rotation curve is seen for most spiral galaxies suggests that there is a common cause for the asymmetry. One possibility is that the asymmetry could arise from ram pressure. Since most galaxies are moving relative to the cosmic medium, it is expected that there will be an enhanced density towards the leading point of the galaxy. This asymmetric density could produce an apparent velocity gradient across the galaxy that could explain the apparent rotation curve. Naturally, there would be range of orientations and the apparent velocity gradient must be added to any intrinsic rotation curve to produce a wide diversity of results. Thus, curvature redshift could explain the galactic rotation curves if there is an asymmetric distribution of material in the galactic halo. Both cosmologies have problems with galactic rotation curves. BB not only requires dark matter but does not have any definite models for its distribution. Curvature cosmology has the problem of achieving sufficient asymmetry to mimic a rotation curve.

2.13 Redshifts in our Galaxy

In our Galaxy, the Milky Way, there is an interesting prediction. The density of the inter-stellar ionized gas is high enough to inhibit curvature redshift for radio frequencies. From Part 3: Eq. 10 it was shown that for wavelengths longer than about $20.6N^{-1/2}$ m the effect of refractive index in fully ionized plasma will inhibit curvature redshift. The refractive index of neutral hydrogen is too low to inhibit curvature redshift. However, any fully ionized plasma with $N > 10^4$ will inhibit curvature redshift for the 21 cm hydrogen line. Since the local interstellar medium has an electron density of about 10^5 m^{-3} (Redfield, 2006), curvature redshift will be inhibited for the 21 cm hydrogen in regions of

the galaxy near the sun. Thus for sight lines close to the Galactic plane we can assume a similar density and thus a similar inhibition with the result that the observed radio redshifts can be correctly interpreted as velocities. Thus, there is little change needed to the current picture of Galactic structure and rotation derived from 21 cm redshifts. However, there may be some curvature redshift present in sight lines away from the plane and especially in the Galactic halo.

Since optical redshifts have the full effects of curvature redshift, it should be possible to find objects with discrepant redshifts where the optical redshift is greater than the radio redshift. The difficulty is that the two types of radiation are produced in radically different environments: the optical in compact high temperature objects, such as stars, and the radio in very low-density cold clouds. In addition, there is the complication that within the galactic plane, optical extinction due to dust limits the optical range to about one kpc.

Curvature redshift may help to explain an old stellar mystery. There is a long history provided by Arp (1992) of observations of anomalous redshifts in bright hot stars, which is called the K-term or K-effect. Allen (1976) states that B_0 stars typically show an excess redshift of 5.1 $\mathrm{m\,s^{-1}}$, A_0 have 1.4 $\mathrm{km\,s^{-1}}$ and F_0 have 0.3 $\mathrm{km\,s^{-1}}$. This can be explained if these stars have a large corona that produces a curvature redshift. It is probably no coincidence that such stars have large stellar winds and mass outflows. In order to see if it is feasible let us consider a simple model for the outflow in which the material has a constant velocity v_0, and conservation of matter (Gauss's Law) then requires that the density has inverse square law dependence. Although this is incorrect at small stellar radii, it is a reasonable approximation further from the star. Then if ρ_1 is the density at some inner radius r_1, then integration of Part 3: Eq. 9 out to

a radius r_2, the expected redshift in velocity units is

$$v = \sqrt{\frac{2G\dot{M}}{v_o}} \log\left(\frac{r_2}{r_1}\right),$$

where $\dot{M}$ is the observed stellar mass-loss-rate. Then with $\dot{M}$ in solar masses per year, with v and v_0 in $\mathrm{km\,s^{-1}}$, the redshift is

$$v = 91.7\sqrt{\frac{\dot{M}}{v_o}} \log\left(\frac{r_2}{r_1}\right) \mathrm{km\,s^{-1}},$$

With $\dot{M} = 10^{-5} M_\odot\,\mathrm{yr}^{-1}$ Cassinelli (1979), $v_0 = 1\,\mathrm{km\,s^{-1}}$ and $r2/r1 = 10^3$ the predicted redshift (in velocity units) is $2\,\mathrm{km\,s^{-1}}$ which is in reasonable agreement with the observed K-effects mentioned above.

2.14 Anomalous redshifts

Arp (1987); Ratcliffe (2010) have argued that there is strong observational evidence for anomalous redshifts between quasars and galaxies. Typically there is a quasar very close to a galaxy with a material bridge or other evidence that suggests that they are associated. Chu et al. (1998) report on five X-ray emitting blue stellar objects located less than $12'$ from the X-ray Seyfert galaxy NGC 3516. In this case the association is that the objects lie close to a straight line on either side of the galaxy and that their redshifts are proportional to $\log(\theta)$ where θ is the angular distance from the central galaxy. Furthermore the line of objects is within a few degrees of the minor axis of NGC 3516. The measured redshifts are 0.33, 0.69, 0.93, 1.4 and 2.1. NGC 3516 is a barred spiral galaxy and it has a redshift of 0.00884.

Can CC explain this redshift anomaly? If the objects are seen through a large dense cloud, such as a galactic halo, then curvature redshift will produce an extra redshift due to the photons passage through the cloud. the extra redshift,

δ, is

$$\delta = 1.72 \times 10^{-10} \int \sqrt{N(x)}\, dx,$$

where $N(x)$ is the number density and distances are measured in pc. If z is the cosmological redshift then the extra-observed redshift is $\Delta z = (1+z)(e^{\delta} - 1)$. In order to achieve an extra redshift $\delta \approx 1$ with a distance of 10^4 pc the gas number density must be about 3×10^{11} m^{-3}. Now although cold interstellar molecular clouds can have densities reaching this value it is still a very high density. But if the size is increased by a factor of two the required density is decreased by a factor of four. Moreover the objects with the largest redshifts are the furthermost away from the galaxy. These redshifts could be explained by curvature redshift in a very large, very dense galactic halo with a hole in the middle. Since NGC 3516 has a very low redshift and is seen nearly face on the implication is that this gas cloud is probably shaped like a torus and it lies in the galactic plane of NGC3516. A further test is to compare an estimate of the mass of this torus with that for a typical galaxy. Since a torus formed by the rotation of a circle with radius r about a axis in the plane of the circle where the radius of rotation is R, its volume is $V = 2\pi^2 R r^2$. With R and r in kpc and an average density of N its mass is $M = 0.484 R r^2 N\, M_{\odot}$. Then with $R = 15\,\text{kpc}$, $r = 10\,\text{kpc}$ and $N = 3 \times 10^{11}$ the mass is $2 \times 10^{14} M_{\odot}$ which considerably larger than a normal galaxy. Since these anomalous redshifts are completely outside any BB model the only reason that these observations are not fatal to BB is their the controversial nature.

2.15 Voids

If CC is valid then the redshift of the galaxies in the Coma cluster (Section 2.6) will have been increased, on average, by the additional redshift due to the inter-galactic gas. Thus, they will have, on average, a larger redshift than an isolated galaxy at the same distance. Table 8 shows the predicted (effective) velocity for a galaxy in the center plane of the Coma cluster as a function of the projected radius. The second column is the velocity at that exact radius and the third column shows the average velocity of galaxies (uniformly spread in area) within that radius. This simulation also showed that the average velocity offset for the galaxies in the Coma cluster is 1206 kms^{-1} which means that the redshift of the center of the Coma cluster is 6926-1206=5720 kms^{-1}. This offset is important for calculating the Hubble constant which from these figures is 5270/87.1=65.7 $\mathrm{kms}^{-1}\,\mathrm{Mpc}^{-1}$.

In addition, the redshift of objects seen through a cluster will be increased by curvature-redshift from the inter-galactic gas. Karoji, Nottale & Vigier (1976) claim to have seen this effect. They examined radio galaxies and classified them into region A if their light does not pass through a cluster and region B if their light passes through a cluster. They found no significant differences in magnitudes between the two regions but they did find a significant difference in the average redshifts that was consistent over the complete range. Their result is that radio galaxies seen through a cluster had an average extra redshift (in velocity units) of 2412±1327 $\mathrm{km\,s}^{-1}$. Overall the difference in the distance modulus was $\mu = 0.16 \pm 0.04$, which is just significant. Since the density and distribution of the gas in the clusters is unknown and the limiting radius of the cluster is not stated it is impossible to get an accurate prediction. Nevertheless,

Table 8: Velocity at, and average velocity within various projected radii in the Coma cluster (distance = 87.1 Mpc).

Radius[a] /Mpc	Velocity /km s^{-1}	Mean velocity /km s^{-1}
0.0	2327.7	2327.7
0.5	1477.7	1764.8
1.0	1033.4	1342.5
1.5	803.3	1096.9
2.0	658.6	933.2
2.5	557.0	814.4
3.0	481.0	723.3
3.5	421.7	650.7
4.0	374.0	541.2
4.5	334.8	541.2
5.0	302.0	498.7

[a]projected radius

we note that for the Coma cluster with a radius of 2 Mpc the average extra redshift (from Table 8 with a factor of two) corresponds to 1866 $\mathrm{km\,s^{-1}}$ showing that curvature-cosmology could explain the effect. In a different study, Nottale (1976) and Nottale & Vigier (1977) compared the magnitude of the brightest galaxy in a cluster with that in another cluster with similar redshift. They found that there was no significant difference in magnitudes between clusters but that the clusters with the largest number of galaxies had the higher redshift difference between the pairs. On average the redshift difference (in velocity units) was 292 ± 85 $\mathrm{km\,s^{-1}}$. This can be explained by the expected correlation between number of galaxies and size and density of the inter-galactic gas. However it should be noted that these observations have been disputed by Rood & Struble (1982).

In his review of voids in the distribution of galaxies, Rood (1988) quotes Mayall (1960) who observed a large void in the distribution of galaxies in front of the Coma cluster. This void has a magnitude of about 3000 $\mathrm{kms^{-1}}$, which although somewhat larger, is not inconsistent with the expected value of about 1200 $\mathrm{km\,s^{-1}}$. In other words, the Coma cluster galaxies have an extra curvature-redshift due to the inter-galactic gas. However, the galaxies just outside the cluster nearer to us do not have this extra redshift and would appear to be closer to us. Hence, we see an apparent void in the redshift distribution in front of the Coma cluster.

A consequence of gas clouds and curvature-redshift is that the distribution of redshifts is similar to but not identical to the distribution of z distances. Galaxies that are behind a cloud will have a higher redshift than would be expected from a simple redshift distance relationship. Thus, we would expect

to see anomalous voids and enhancements in the redshift distribution. This will be accentuated if the gas clouds have a higher than average density of galaxies. de Lapparent, Geller & Huchra (1986) show a redshift plot for a region of the sky that includes the Coma cluster. Their data are from the Center for Astrophysics redshift survey and their plot clearly shows several voids. They suggest that the galaxies are distributed on the surfaces of shells. However, this distribution could also arise from the effects of curvature-redshift in clouds of gas.

3 Conclusion

Results for the topics of the Hubble redshift, X-ray background radiation, the cosmic background radiation and dark matter show strong support for curvature cosmology. In particular CC predicts that the Hubble constant is $64.4 \pm 0.2\,\mathrm{km\,s^{-1}\,Mpc^{-1}}$ whereas the value estimated from the type 1a supernova data is $63.8 \pm 0.5\,\mathrm{kms^{-1}\ Mpc^{-1}}$ and the result from the Coma cluster (Section 2.15) is $65.7\,\mathrm{kms^{-1}\ Mpc^{-1}}$. In CC the theoretical cosmic temperature is 2.56×10^9 K for the cosmic gas and the temperature estimated from fitting the X-ray data is $(2.62 \pm 0.04) \times 10^9$ K. The predicted temperature for the CMBR is 3.18 K. whereas Mather et al. (1990) measured the temperature to be 2.725 K. This prediction does depend on the nuclei mix in the cosmic gas and could vary from this value by several tenths of a degree. Curvature cosmology does not need dark matter to explain the velocity dispersion in clusters of galaxies or the shape of galactic rotation curves.

Other topics in this part namely the Sunyaev–Zel'dovich effect, gravitational lens, the Gunn–Peterson trough, redshifts in our Galaxy and voids can be ex-

plained by CC or are fully compatible with CC. Currently CC provides a qualitative explanation for the abundances of light elements (the 'primordial' abundances) but not quantitative predictions. The remaining topics in Section 2 namely Lyman-α forest, galaxy rotation and anomalous redshift are compatible but with some problems.

Curvature pressure can explain the non-cosmological topic of solar neutrino production but since this already explained by neutrino oscillations it must remain a curiosity. The explanation of the *Pioneer* 10 anomalous acceleration is feasible if the inter-planetary dust density is a little larger than current estimates.

Acknowledgments

This research has made use of the NASA/IPAC Extragalactic Database (NED) that is operated by the Jet Propulsion Laboratory, California Institute of Technology, under contract with the National Aeronautics and Space Administration. The calculations have used Ubuntu Linux and the graphics have used the DISLIN plotting library provided by the Max-Plank-Institute in Lindau.

References

Abramowitz M. & Stegun, I.A., (1972)., Handbook of Mathematical Functions, New York, Dover.

Allen, C. W., (1976), Astrophysical Quantities, 3rd Ed , London, Athlone.

Arp, H., (1987). Quasars, Redshifts and Controversies, Berkeley, Interstellar Media.

Arp, H., (1992). Redshifts of high-luminosity stars - The K effect, the Trumpler effect and mass-loss corrections. MNRAS, 258, 800.

Battistelli, E. S., De Peter, M., Lamagna, L., Melchiorre, F., Palladino, E., Savini, G, Cooray, A., Melchiorre, A., Rephaeli, Y. & Shimin, M., (2002). Cosmic Microwave Background Temperature at Galaxy Clusters. Astrophysical Journal, 580, L104

Becker, R. H., Fan, X., White, R.L.,Strauss, M.A., Narayanan, V.K., Lupton, R. H., Gunn, J. E., Annis, J., Bahcall, N. A., Brinkmann, J., Connolly, A. J., Csabal, I., Czarapata, P. C., Doi, M., Heckman, T. M., Hennsy, G. S., Ivezić,Ž., Knapp, G. R., Lamb, D. Q., McKay, T. A., Munn, J. A., Nash, T., Nichol, R., Pier, J. R., Richsrds, G. T., Schneider, D. P., Stoughton, C., Szalay, A. S., Thakar, A. R. & York, D. G., (2001). Evidence for Reionization at z 6: Detection of a Gunn-Peterson Trough in a z=6.28 Quasar. Astrophysical Journal, 122, 2850.

Beijersbergen, M. (& van der Hulst, J.M.,) 2004, Phd Thesis, University of Groningen.

Bielby, R.M. & Shanks, T., (2007). Anomalous SZ contribution to three-year WMAP data. MNRAS, 382, 1196.

Briel, U.G., Henry, J.P. & Bhringer, H., (1992). Observation of the Coma cluster of galaxies with ROSAT during the all-sky survey. Astronomy and Astrophysics, 259, L31.

Cabre, A., Gaztaaga, E., Manera, M., Fosalba, P. & Castander, F., (2006). Cross-correlation of Wilkinson Microwave Anisotropy Probe third-year data and the Sloan Digital Sky Survey DR4 galaxy survey: new evidence for dark energy. MNRAS, 372, L23.

Cassinelli, J.P., (1979). Stellar winds. Annual Review of Astronomy and Astrophysics, 17, 275.

Chu, Y., Wei, J., Hu, J., Zhu, X & Arp, H., (1998). Quasars around the Seyfert Galaxy NGC 3516. Astrophysical Journal, 5007, 596.

Colless, M. & Dunn, A.M., (1996). Structure and Dynamics of the Coma Cluster. Astrophysical Journal, 458, 435.

Cowsik, R. & Kobetich, E.J., (1972). Comment on Inverse Compton Models for the Isotropic X-Ray Back-Ground and Possible Thermal Emission from a Hot Intergalactic Gas. Astrophysical Journal, 177, 585.

de Groot, S.R., Leeuwen, W.A. & van Weert, C.G., (1980). Relativistic Kinetic Theory, Amsterdam, North-Holland.

Dennis, B.R., Suri, A.N. & Frost, K.J., (1973). The Diffuse X-Ray Spectrum from 14 TO 200 keV as Measured on OSO-5. Astrophysical Journal, 186. 97.

de Lapparent, V., Geller, M.J. & Huchra, J.P., (1986). A slice of the universe. Astrophysical Journal, 302, L1.

Ellis, G. G. R., (1984). Alternatives to the Big Bang. Annual Review of Astronomy and Astrophysics, 22, 157.

Field, G.B. & Henry, R.C., (1964). Free-Free Emission by Intergalactic Hydrogen.. Astrophysical Journal, 140, 1002.

Finoguenov, A., Briel, U.G., Henry, J.P., Gavazzi, G., Iglesias-Paramo, J. & Boselli, A., (2004). The X-ray luminosity function of galaxies in the Coma cluster. Astronomy and Astrophysics, 419, 47.

Fixsen, D.J., Cheng, E.S., Gales, J.M., Mather, J.C., Shafer, R.A. & Wright, E.L., (1996). The Cosmic Microwave Background Spectrum from the Full COBE FIRAS Data Set. Astrophysical Journal, 473, 576.

Freedman, W. L., Madore, B. F., Gibson, B. K., Ferrarese, L., Kelson, D. D., Sakai, S., Mould, J.R., Kennicutt, R. C. Jr., Ford, H. C., Graham, J. A., Huchra, J. P., Hughes, S. M. G., Illingwoth, G. D., Macri, L. M. & Stetson, P. B., (2001). Final Results from the Hubble Space Telescope Key Project to Measure the Hubble Constant. Astrophysical Journal, 553, 47.

Fukada, Y., Hayakawa, S., Ikeda, M., Kasahara, J., Makino, F. & Tanaka, Y., (1975). Rocket observation of energy spectrum of diffuse hard X-rays. Astrophys. Space Sci., 32, L1.

Ge, J., Bechtold, J. & Black, J.H., (1997). A New Measurement of the Cosmic Microwave Background Radiation Temperature at Z = 1.97. Astrophysical Journal, 474, 67.

Giacconi, R., Gursky, H., Paolini, F.R. & Rossi, B.B., (1962). Evidence for x Rays From Sources Outside the Solar System. Phys. Rev. Letters, 9, 439.

Goldstein, H., (1980). Classical Mechanics, Massachusetts, Addison-Wesley.

Gould, R.J. & Burbidge, G.R., (1963). X-Rays from the Galactic Center, External Galaxies, and the Intergalactic Medium. Astrophysical Journal, 138, 969.

Gruber, D.E., Matteson, J.L. & Peterson, L.R., (1999). The Spectrum of Diffuse Cosmic Hard X-Rays Measured with HEAO 1. Astrophysical Journal, 520, 124.

Gunn, J.E. & Peterson, B.A., (1965). On the Density of Neutral Hydrogen in Intergalactic Space. Astrophysical Journal142, 1633.

Holt, S.S.,1992, in The X-ray Background, ed. X. Barcons & A. C. Fabian, Cambridge University Press, 29

Horstman-Morretti, E., Fuligni, F., Horstman, H.M. & Brini, D., (1974). A New Rocket Measurement on the Diffuse X-Ray Background. Astrophys. Space Sci., 27, 195.

Hoyle, F. & Narlikar, J.V., (1962). A New Theory of Gravitation. Royal Society of London Proceedings Series A, 282,191.

Hughes, J. P., (1989). The mass of the Coma Cluster - Combined X-ray and optical results. Astrophysical Journal, 337, 21

Itoh, N., Sakamoto, T., Kusano, S., Nozawa, S. & Kohyama, Y., (2000). Relativistic Thermal Bremsstrahlung Gaunt Factor for the Intracluster Plasma. II. Analytic Fitting Formulae. Astrophysical Journal Supplement, 128, 125.

Karoji, K., Nottale, L. & Vigier, J.-P., (1976). A peculiar distribution of radial velocities of faint radio-galaxies with corrected apparent magnitudes between 13.0 and 15.5. Astrophys., Space Sci., 44, 229.

Kinzer, R.L., Jung, G.V., Gruber, D.E., Matterson, J.L. & Peterson, L.E., (1997). Diffuse Cosmic Gamma Radiation Measured by HEAO 1. Astrophysical Journal, 475, 361.

Lieu, R., Mittaz, J.P.D. &Zhang, S.-N., (2006). The Sunyaev-Zel'dovich Effect in a Sample of 31 Clusters: A Comparison between the X-Ray Predicted and WMAP Observed Cosmic Microwave Background Temperature Decrement. Astrophysical Journal, 648, 176.

Lima, J.A.S., Silva, A.J. & Viegas, S.M., (2000). Is the radiation temperature-redshift relation of the standard cosmology in accordance with the data? MNRAS, 312, 747.

Liu, M.C. & Graham, J.R., (2001). Infrared Surface Brightness Fluctuations of the Coma Elliptical Galaxy NGC 4874 and the Value of the Hubble Constant. Astrophysical Journal, 557, L31.

Longair, M.S., (1991). Theoretical Concepts in Physics, Cambridge University Press.

Mandrou, P., Vedrenne, G. & Niel, M., (1979). Diffuse cosmic gamma-ray observations from 0.3 to 6 MeV in two regions near the Galactic center and anticenter. Astrophysical Journal, 230, 97.

Marshall, F.E., Boldt, S.S., Miller, R.B., Mushotzky, R.F., Rose, L.A., Rothschild, R.E. & Sermlemitios, P.J., (1980). The diffuse X-ray background spectrum from 3 to 50 keV. Astrophysical Journal, 235, 4.

Mather, J. C., Cheng, E. S., Epler, Jr., R. E., Isaacmsn, R. B., Meyer, S. S., Shafer, R. A., Wiess, R., Wright, E. L., Bennett, C. L., Boggess, N. W., Dwek, E., Gulkis, S., Hauser, M. G., Janssen, M., Kelsall, T., Lubin, P. M., Moseley, S. H., Murdock, T. L., Silverberg, R. F., Smoot, G. F. & Wilkinson, D. T., (1990). A preliminary measurement of the cosmic microwave

background spectrum by the Cosmic Background Explorer (COBE) satellite. Astrophysical Journal, 354, L37.

Mayall, N.U., (1960). Advantages of electronic photography for extragalactic spectroscopy. Annales d'Astrophysique, 23, 344.

Mazets, E.P., Golenetskii, S.V., Il'inskii, V.N., Gur'yan, Yu.A. & Kharitonova, T.V., (1975). Diffuse cosmic gamma-ray background in the 28 keV-4.1 MeV range from Kosmos 461 observations. Astrophys. Space Sci., 33, 347.

Nottale, L., (1976). Redshift Anomaly in Associations of Clusters of Galaxies?. Astrophysical Journal, 208, L103.

Nottale, L. & Vigier J.P., (1977). Continuous increase of Hubble modulus behind clusters of galaxies. Nature, , 268, 608

Nozawa, S., Itoh, N. & Kohyama, Y., (1998). Relativistic Thermal Bremsstrahlung Gaunt Factor for the Intracluster Plasma. Astrophysical Journal, 507, 530.

Peebles, P.J.E., (1993). Principles of Physical Cosmology, New Jersey, Princeton.

Peng Oh, S. & Furlanetto, R., (2005). How Universal is the Gunn-Peterson Trough at z 6. Astrophysical Journal, 620, L9.

Pettini, M., Hunstead, R.W., Smith, L.J. & Mar, D.P., (1990). The Lyman-Alpha Forest at 6KM/S-1 Resolution. MNRAS, 246, 545.

Ratcliffe, H., (2010). Anomalous Redshift Data and the Myth of Cosmological Distance. /joc, 413, 109

Rauch, M., (1998). The Lyman Alpha Forest in the Spectra of QSOs. Annual Review of Astronomy and Astrophysics, 36, 267.

Redfield, S., (2006). The Local Interstellar Medium. ASPC, 352, 79.

Rood, H.J. & Struble, M.F., (1982). Test for a richness-dependent component in the systemic redshifts of galaxy clusters. /apj, 252, L7.

Rood, H.J., (1988). Voids. Annual Review of Astronomy and Astrophysics, 26, 245.

Roth, K.C. & Meyer D.M., (1995). Cyanogen excitation in diffuse interstellar clouds. Astrophysical Journal, 441, 129.

Srianand, R., Petitjean, P. & Ledoux, C., (2000). The cosmic microwave background radiation temperature at a redshift of 2.34. Nature408, 931.

Srianand, R., Noterdaeme, P., Ledoux, C. & Petitjean, P, (2008). First detection of CO in a high-redshift damped Lyman-? system. Astronomy and Astrophysics, 482L, 39.

Sunyaev, R.A., (1980). The Microwave_Background Radiation in the Direction Toward Clusters of Galaxies. Soviet Astronomy Letters, 6, 213.

Sunyaev, R.A. & Zel'dovich, Ya.B., (1970). Small-Scale Fluctuations of Relic Radiation. Astrophys. Space Sci. 7, 3.

Tolman, R.C., (1934). Relativity, Thermodynamics and Cosmology, Oxford University Press.

Trombka, J.L., Dyer, C.S., Evans, L.G., Bielefeld, M.J., Seltser, S.M. & Metzger, A.E., (1977). Reanalysis of the Apollo cosmic gamma-ray spectrum in the 0.3 to 10 MeV energy region. Astrophysical Journal, 212, 925.

Watt, M.P., Ponman, T.J., Bertram, D., Eyles, C.J., Skinner, G.K. & Willmore, A.P., (1992). The morphology and dark matter distribution of the Coma cluster of galaxies from X-ray observations. MNRAS, 258, 738.

White, R.L., Becker, R.H., Helfand, D.J. & Gregg, M.G., (1997). A Catalog of 1.4 GHz Radio Sources from the FIRST Survey. Astrophysical Journal, 475, 479.

White, R. L., Becker, R.H., Fan, X. & Strauss, M.A., (2005). Hubble Space Telescope Advanced Camera for Surveys Observations of the z = 6.42 Quasar SDSS J1148+5251: A Leak in the Gunn-Peterson Trough. /aj, 129, 2102.

White, S.D.M., Briel U.G., Henry J.P., (1993). X-ray archaeology in the Coma cluster. MNRAS, 261, L8.

Zwicky, F. 1937. On the Masses of Nebulae and of Clusters of Nebulae. Astrophysical Journal, 86, 217.